The Journal of Chemical Physics

Electronic structure calculations in electrolyte solutions: Methods for neutralization of extended charged interfaces

Cite as: J. Chem. Phys. **153**, 124101 (2020); https://doi.org/10.1063/5.0021210
Submitted: 08 July 2020 . Accepted: 09 September 2020 . Published Online: 22 September 2020

Arihant Bhandari, Lucian Anton, Jacek Dziedzic, Chao Peng, Denis Kramer, and Chris-Kriton Skylaris

The Journal of Chemical Physics ARTICLE scitation.org/journal/jcp

Electronic structure calculations in electrolyte solutions: Methods for neutralization of extended charged interfaces

Cite as: J. Chem. Phys. 153, 124101 (2020); doi: 10.1063/5.0021210
Submitted: 8 July 2020 • Accepted: 9 September 2020 •
Published Online: 22 September 2020

Arihant Bhandari,[1,2] Lucian Anton,[3] Jacek Dziedzic,[1,2,4] Chao Peng,[2,5] Denis Kramer,[2,5,6] and Chris-Kriton Skylaris[1,2,a)]

AFFILIATIONS

[1]School of Chemistry, University of Southampton, Highfield, Southampton SO17 1BJ, United Kingdom
[2]The Faraday Institution, Quad One, Becquerel Avenue, Harwell Campus, Didcot OX11 0RA, United Kingdom
[3]CCFE, Culham Science Centre, Abingdon, United Kingdom
[4]Faculty of Applied Physics and Mathematics, Gdańsk University of Technology, Gdańsk 80-233, Poland
[5]Engineering Sciences, University of Southampton, Southampton SO17 1BJ, United Kingdom
[6]Helmut-Schmidt-University, University of the Armed Forces, 22043 Hamburg, Germany

[a)]**Author to whom correspondence should be addressed:** C.Skylaris@soton.ac.uk

ABSTRACT

Density functional theory (DFT) is often used for simulating extended materials such as infinite crystals or surfaces, under periodic boundary conditions (PBCs). In such calculations, when the simulation cell has non-zero charge, electrical neutrality has to be imposed, and this is often done via a uniform background charge of opposite sign ("jellium"). This artificial neutralization does not occur in reality, where a different mechanism is followed as in the example of a charged electrode in electrolyte solution, where the surrounding electrolyte screens the local charge at the interface. The neutralizing effect of the surrounding electrolyte can be incorporated within a hybrid quantum–continuum model based on a modified Poisson–Boltzmann equation, where the concentrations of electrolyte ions are modified to achieve electroneutrality. Among the infinite possible ways of modifying the electrolyte charge, we propose here a physically optimal solution, which minimizes the deviation of concentrations of electrolyte ions from those in open boundary conditions (OBCs). This principle of correspondence of PBCs with OBCs leads to the correct concentration profiles of electrolyte ions, and electroneutrality within the simulation cell and in the bulk electrolyte is maintained simultaneously, as observed in experiments. This approach, which we call the Neutralization by Electrolyte Concentration Shift (NECS), is implemented in our electrolyte model in the Order-*N* Electronic Total Energy Package (ONETEP) linear-scaling DFT code, which makes use of a bespoke highly parallel Poisson–Boltzmann solver, DL_MG. We further propose another neutralization scheme ("accessible jellium"), which is a simplification of NECS. We demonstrate and compare the different neutralization schemes on several examples.

I. INTRODUCTION

Density functional theory (DFT) provides valuable insights into material properties and phenomena at the atomic scale starting from just the knowledge of the structural arrangement of atoms and molecules. Due to its *ab initio* nature, it is extensively used in physical and chemical sciences to model complex material systems. The systems can be structurally very complex such as protein–ligand systems, nanoparticles, and electrode–electrolyte interfaces, which can involve tens of thousands of atoms. Conventional DFT scales as $O(N^3)$, where N is the number of atoms, which makes it prohibitively costly to model such large complex systems. DFT has been reformulated in terms of the single particle density matrix to scale linearly with the number of atoms as in the Order-*N* Electronic Total Energy Package (ONETEP).[1]

Apart from structural complexity, in many applications, such as in biology, electrochemistry, energy conversion, and storage, the systems under consideration have a net non-zero charge. Under

periodic boundary conditions (PBCs), the electrostatic potential of a charged system diverges, making it necessary to neutralize the overall charge. Traditional DFT approaches introduce a uniform background charge ("jellium") to neutralize the charged system, which introduces spurious charge densities and unphysical energies, whereas, in reality, electroneutrality is maintained by the surrounding electrolyte solution.

The surrounding electrolyte solution can be included mainly via explicit solvation,[2] implicit solvation,[3] or both.[4] In the former, explicit molecules of the surrounding solvent and electrolyte are added and considered on an equal footing as the main system. The surrounding electrolyte molecules not only neutralize but can also form bonds and adsorb on the main system.[5] More extensive models of electrode–electrolyte interfaces can also include an explicit counter-electrode.[6,7] While consideration of the explicit solvent and electrolyte molecules helps in describing local bonding effects and the local effects of electric field,[8] it drastically increases the configurational degrees of freedom. Sampling this large configurational space leads to an increase in the computational overhead and the loss of focus on the main system.

In many cases, one is focused in the main system and only needs a mean-field neutralizing effect of the surrounding electrolyte solution. In such a scenario, implicit models of electrolyte solutions are useful as they divide the system into two subsystems: an explicit quantum subsystem whose degrees of freedom are retained and a continuum model for the surrounding electrolyte solution, which averages out the degrees of freedom of the electrolyte solution.[9,10] One can retain a first solvation shell of the bonding solvent and electrolyte molecules, while using an implicit description for the surrounding solution, to reduce computational cost, without missing important physics. These hybrid quantum–continuum models are based on solving the Poisson–Boltzmann equation (P–BE).[11] Many DFT+P–BE models have been developed recently.[12–18]

Several approaches to electroneutrality have been proposed in DFT+P–BE models,[16] among which the jellium approach where a uniform neutralizing background charge is introduced to ensure electroneutrality is widely used.[19] Jellium, however, does not locally screen the charge on surfaces exposed to the electrolyte solution and could result in unphysical estimates of the energetics and other properties. Another approach is to modify the concentrations of Boltzmann ions in order to ensure electroneutrality. This is done by setting the chemical potentials of Boltzmann ions to satisfy the electroneutrality constraint.[16] Often anti-symmetric excess chemical potentials of Boltzmann ions are assumed, an approach known as Donnan neutralization, which has been found in membrane equilibria.[20] This approach has been implemented within several DFT packages.[13,16] Another approach to electroneutrality in simulations of charged interfaces is the effective screening method (ESM), where the boundary conditions are modified to make the slab non-periodic in the direction of the surface normal with the help of Green's function.[21] In this study, we develop a neutralization scheme by shifting the concentration of electrolyte ions for ensuring electroneutrality in calculations of charged periodic systems via the Poisson–Boltzmann electrolyte model of the ONETEP linear-scaling DFT code.[18]

We present and study the properties of a model in which electroneutrality is achieved by shifting the average concentrations of the electrolyte ions from the asymptotic values corresponding to the open system. For a large enough simulation cell, we show that there is an optimal average concentration shift, which minimizes the differences between the space-dependent electrolyte ion concentrations associated with periodic and open boundary conditions (OBCs). Subsequently, we show that the linear approximation of this method leads to a new type of jellium neutralization. In Secs. II–IV, we describe the background of the computational tools, theory, implementation details, and results of tests on several finite and extended charged extended systems.

II. BACKGROUND OF COMPUTATIONAL TOOLS AND METHODS

A. The ONETEP linear-scaling DFT program

The electronic structure is computed with the ONETEP linear-scaling DFT program,[1] where Kohn–Sham DFT has been reformulated in terms of the single particle density matrix,[22] $\rho_e(\mathbf{r},\mathbf{r}') = \phi_\alpha(\mathbf{r})K^{\alpha\beta}\phi^*_\beta(\mathbf{r}')$. Here, the matrix $\mathbf{K}$ is called the "density kernel," $\{\phi_\alpha\}$ are the localized orbitals, called the Non-orthogonal Generalized Wannier Functions (NGWFs),[23] and there is implied summation over repeated Greek indices (α and β). During the computation procedure, the NGWFs and the density kernel are self-consistently optimized via two nested loops. Within these loops, the electrostatic potential associated with the total charge distribution, made up of the quantum system and the electrolyte charges, is solved for with DL_MG, as described in Sec. II B. The NGWFs are expressed in a basis set comprised of periodic sinc (psinc) functions,[23,24] which, being equivalent to a plane-wave basis set, are controlled by a single kinetic energy cutoff parameter.

We demonstrate the linear-scaling behavior of ONETEP on a periodic bulk graphite system and compare the computational time with a conventional plane-wave DFT code as, shown in Fig. 1. We clearly see linear-scaling behavior with ONETEP[1] and cubic-scaling with a conventional plane-wave DFT code. As evident, a large calculation of up to 20 000 atoms can be performed in less than a day's time with linear-scaling ONETEP, while such calculations are outside the regime of feasibility of a conventional plane-wave DFT code. This demonstrates the suitability of ONETEP for complex material systems such as electrode–electrolyte interfaces and protein–ligand systems.

B. The DL_MG Poisson–Boltzmann solver library

DL_MG is a bespoke parallel solver (MPI+OpenMP) for P–BE and the Poisson equation described in detail in Refs. 25 and 26. DL_MG has been interfaced with several other DFT packages such as CASTEP[27] and PSI4.[28] The discretization is done on a regular grid, the nonlinear P–BE is solved with a global inexact Newton method,[29] and the linear Poisson-type equations are solved with a parallel multigrid method. The higher-order corrections for the finite difference derivatives are computed with a defect correction iterative procedure.[30,31]

The non-linear Boltzmann term, which is of particular interest in this paper, includes an accessibility function that models the short range ion–solute repulsion and the chemical potential, which is needed for periodic boundary conditions as described in Ref. 18.

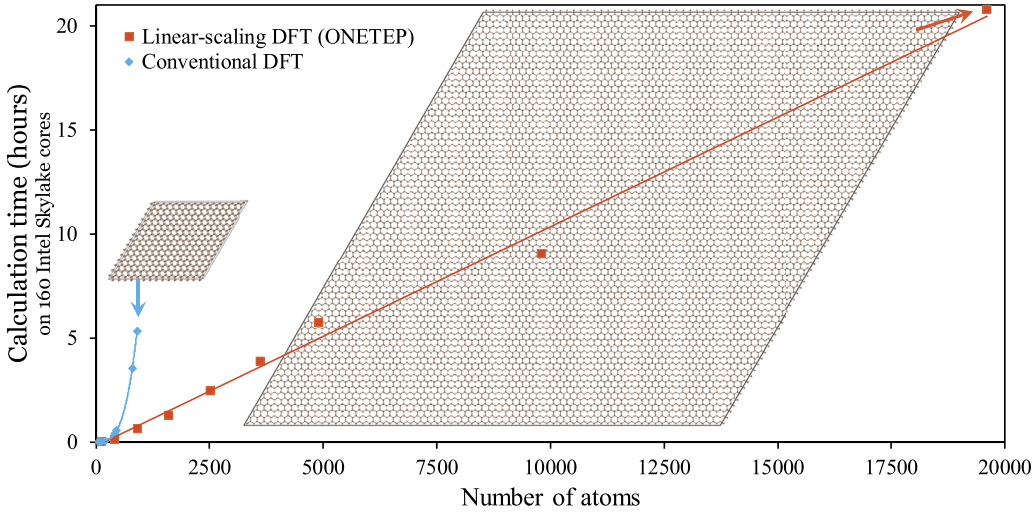

FIG. 1. Comparison of the computational time using the ONETEP linear-scaling DFT code against using a conventional plane-wave DFT code for periodic graphite systems with varying number of atoms. The computations were performed on the Iridis 5 supercomputer at the University of Southampton on 40 MPI processes with 4 OpenMP threads each (160 cores in total).

III. THEORY

Systems studied in this work are composed of a quantum atomistic subsystem with charge density $\rho(\mathbf{r})$ "the solute"[32] in contact with a continuum electrolyte with p distinct ion types with charges $\{z_i\}$ and space-dependent number densities $\{c_i(\mathbf{r})\}$ at temperature T; hence, the electrolyte charge density is defined by $\rho_{\text{mob}}(\mathbf{r}) = \sum_{i=1}^{p} z_i c_i(\mathbf{r})$. The relationship between the total charge distribution and the electrostatic potential $v(\mathbf{r})$ is modeled with the P–BE,

$$\nabla \cdot (\varepsilon(\mathbf{r})\nabla v(\mathbf{r})) = -4\pi\rho_{\text{tot}}(\mathbf{r}), \tag{1}$$

where $\varepsilon(\mathbf{r})$ is the relative permittivity and the total charge density $\rho_{\text{tot}}(\mathbf{r}) = \rho(\mathbf{r}) + \rho_{\text{mob}}(\mathbf{r})$. In the P–BE approach, the ion concentrations follow the Boltzmann distribution

$$c_i(\mathbf{r}) \propto \lambda(\mathbf{r}) \exp(-\beta z_i v(\mathbf{r})), \tag{2}$$

where $\beta = 1/(k_B T)$ is the inverse temperature, k_B is the Boltzmann constant, and $0 \le \lambda(\mathbf{r}) \le 1$ is the ion accessibility function, which accounts for the short range repulsion between ions and solute. In our case, where we have a quantum description for the solute, the permittivity function $[\varepsilon(\mathbf{r})]$ depends on the electronic charge density, which is part of the solute charge distribution, see Ref. 18.

For finite volume solutes, planar or cylindrical structures, the electrolyte extends to infinity in at least one dimension in which the ion concentrations reach their asymptotic values $c_i(\mathbf{r}) \to c_i^{\infty}$, $i = 1, \ldots, p$ for large $|\mathbf{r}|$. Computations done on finite domains represent this type of configurations by using open boundary conditions (OBCs) for the respective dimensions. However, in many cases, numerical computations in a finite domain (or computational cell) of volume V are much simpler if full periodic boundary conditions (PBCs) are used. In this section, we show that one can use a correspondence condition which allows us to map an OBC configuration of interest to a PBC configuration to be used for computation.

An important difference between OBCs and PBCs in systems with charges is the electroneutrality condition that must be satisfied when using PBCs. This can be derived from Eq. (1) by integrating both sides over the volume of the computational cell. The left-hand side integral can be transformed into a surface integral of $\varepsilon(\mathbf{r})\nabla v(\mathbf{r})$, which vanishes due to the opposite signs of the surface normal on the opposite sides of the simulation cell and the periodicity of $\varepsilon(\mathbf{r})\nabla v(\mathbf{r})$. Hence, the volume integral of the total charge density on the right-hand side must also be zero, which gives the following electroneutrality condition:

$$\int_V \rho_{\text{tot}}^{\text{pbc}}(\mathbf{r})\mathrm{d}\mathbf{r} = 0. \tag{3}$$

In PBCs, it is useful to define bulk concentration as the average electrolyte concentration within the electrolyte accessible volume $[V_{\text{acc}} = \int_V \lambda(\mathbf{r})\mathrm{d}\mathbf{r}]$,

$$c_i^{\text{bulk}} V_{\text{acc}} = \int_V c_i(\mathbf{r})\mathrm{d}\mathbf{r} = N_i\,, i = 1, \ldots, p. \tag{4}$$

For cases of electrolytes under confinement such as electrolytes in porous cavity, where there is no contact with an external reservoir of electrolyte, the number of electrolyte particles (N_i) is conserved. For such canonical systems, the electrolyte charge is constrained following the "charge-conserving P–BE."[33,34] This is something which we have considered in our previous paper also[18] by fixing the bulk concentration in PBCs. For this canonical ensemble of electrolyte, one can minimize the free energy functional to get the concentration for electrolyte ions,[18,33,34]

$$c_i(\mathbf{r}) = c_i^{\text{bulk}} \lambda(\mathbf{r}) \exp(-\beta v(\mathbf{r}) + \beta\mu_i^{\text{ex}})\,, i = 1, \ldots, p, \tag{5}$$

where $\{\mu_i^{\text{ex}}\}$ is the excess chemical potential obtained from conservation of ions in the canonical ensemble [Eq. (4)]. Because the electrolyte is neutral (i.e., $\sum_i^p z_i c_i^{\text{bulk}} = 0$), one has to compensate

the solute charge in this case in order to satisfy Eq. (3). One of the most common solutions to this problem, borrowed from solid state physics, is to add to the system a uniform neutralizing background charge ("jellium"),

$$\rho_{\text{tot}}^{\text{pbc-jellium}}(\mathbf{r}) = \rho_{\text{tot}}(\mathbf{r}) - \frac{1}{V}\int_V \rho_{\text{tot}}(\mathbf{r}')\mathrm{d}\mathbf{r}'. \tag{6}$$

As mentioned in Sec. I, using jellium neutralization for a system that does not have a "natural" neutralization background could introduce spurious biases in the results.

A. Neutralization by electrolyte concentration shift (NECS)

Our approach is based on the following observation: In a solute–electrolyte system with OBCs, a change in the solute charge induces a response in the electrolyte which will transfer to infinity an amount of the like charge and bring in from infinity an amount of opposite charge through the open boundaries of the computational cell in order to reach the new equilibrium. In the case of PBCs, if the solute charge changes, the electroneutrality condition requires the addition of a compensating charge into the computational cell, which can be done in several ways as discussed in Sec. I.

An alternative, more natural approach to electroneutrality in PBCs is to add ions of opposite solute charge and to remove ions with like solute charge, thus mimicking the charge transfers that take place in OBCs but with the constraint to preserve the electroneutrality of the computational cell. The shifted ion concentrations $\{c_i^{\text{bulk}}\}$ must satisfy the electroneutrality condition, which can be expressed as follows:

$$\begin{aligned}\int_V \rho_{\text{mob}}(\mathbf{r})\mathrm{d}\mathbf{r} + \int_V \rho(\mathbf{r})\mathrm{d}\mathbf{r} = 0,\\ \sum_{i=1}^{p} z_i \int_V c_i(\mathbf{r})\mathrm{d}\mathbf{r} + Z_s = 0,\\ \sum_{i=1}^{p} z_i c_i^{\text{bulk}} + Z_s/V_{\text{acc}} = 0.\end{aligned} \tag{7}$$

We link the shifted electrolyte average ion concentrations, $\{c_i^{\text{bulk}}\}$, to the asymptotic value of concentrations in the open system $\{c_i^{\infty}\}$ via the shift parameters $\mathbf{x} = \{x_i\}$,

$$c_i^{\text{bulk}} = c_i^{\infty} - x_i\frac{Z_sC_s}{z_i}, i = 1,\ldots,p, \tag{8}$$

$$\sum_{i=1}^{p} x_i = 1, \tag{9}$$

where we introduce the solute "average concentration" defined as $C_s = 1/V_{\text{acc}}$ for the sake of a uniform notation. The constraint on $\{x_i\}$, Eq. (9), ensures the electroneutrality condition $\sum_i^p z_i c_i^{\text{bulk}} + Z_sC_s = 0$, keeping in mind that the OBC uniform electrolyte is neutral as well, i.e., $\sum_{i=1}^{p} z_i c_i^{\infty} = 0$.

There are an infinite number of combinations in which the electrolyte components can be mixed to achieve electroneutrality. Physical intuition guides us to select the one that would generate spatial distributions of the ion concentrations with the smallest deviation from their OBC counterpart. A suitable mathematical measure of the deviation between OBCs and PBCs is the L_2 square norm of the concentration differences

$$\Delta^2 = \sum_{i=1}^{p}\int_{V(S)} (c_i^{\text{OBC}}(\mathbf{r}) - c_i^{\text{PBC}}(\mathbf{r}))^2\mathrm{d}\mathbf{r} \tag{10}$$

taken over the volume of the computation cell in the case of a finite solute (or over the open boundary in the case of planar structure). However, from the computational complexity point of view, this quantity is impracticable because its minimization would require repeated calls to ONETEP to compute the needed concentrations at various values of the shift parameters $\{x_i\}$ until Δ^2 is minimized. In addition, for certain configurations, the OBCs solution might not be available.

We propose an alternative way of finding the optimal shift parameters, $\{x_i\}$, which can be incorporated into the P–BE solver,[26] and we compare the two methods for several cases. We start from the observation that in OBCs, the concentration profiles given by the classical Boltzmann theory,

$$c_i(\mathbf{r}) = c_i^{\infty}\lambda(\mathbf{r})e^{-\beta z_i v(\mathbf{r})}, \; i = 1,\ldots,p, \tag{11}$$

satisfy the following relationship:

$$\frac{c_i(\mathbf{r})^{\frac{1}{z_i}}}{c_j(\mathbf{r})^{\frac{1}{z_j}}} = \frac{[c_i^{\infty}]^{\frac{1}{z_i}}}{[c_j^{\infty}]^{\frac{1}{z_j}}} \tag{12}$$

in the region fully accessible to the electrolyte, where $\lambda(\mathbf{r}) = 1$. For the PBC case, one can use this relationship as a condition to determine the shift parameters $\{x_i\}$. Using Eqs. (5) and (12), we can derive the following correspondence condition, for PBCs:

$$\frac{1}{z_i}\ln\left(\frac{c_i^{\text{bulk}}e^{\beta\mu_i^{\text{ex}}}}{c_i^{\infty}}\right) = \frac{1}{z_j}\ln\left(\frac{c_j^{\text{bulk}}e^{\beta\mu_j^{\text{ex}}}}{c_j^{\infty}}\right) = \ln X, \tag{13}$$

where X is an arbitrary positive constant. Using Eq. (8), we get for the optimal parameters $\{x_i \equiv x_i^{\text{opt}}\}$,

$$x_i \equiv x_i^{\text{opt}} = \frac{z_ic_i^{\infty}}{Z_sC_s}(1 - e^{-\beta\mu_i^{\text{ex}}}X^{z_i}), \; i = 1,\ldots,p. \tag{14}$$

The constant X can be found from Eq. (9), which can be written as follows:

$$\sum_{i}^{p} z_ic_i^{\infty}e^{-\beta\mu_i^{\text{ex}}}X^{z_i} + Z_sC_s = 0. \tag{15}$$

Eq. (13) can be solved analytically in the linear approximation, which is valid for small Z_sC_s. Expanding the logarithm around 1, we get

$$x_i^{\text{lin}} = -\frac{z_i^2c_i^{\infty}}{Z_sC_s}\ln X + \frac{\beta\mu_i^{\text{ex}}z_ic_i^{\infty}}{Z_sC_s}, \quad i = 1,\ldots,p, \tag{16}$$

and from the constrain condition, Eq. (9), we find

$$\ln X = \frac{\sum_j^p \beta\mu_j^{\text{ex}}z_jc_j^{\infty} - Z_sC_s}{\sum_j^p z_j^2c_j^{\infty}}, \tag{17}$$

which are combined to find the linear approximation

$$\begin{aligned}x_i^{\text{lin}} = &\frac{z_i^2c_i^{\infty}}{\sum_j^p z_j^2c_j^{\infty}}\left(1 - \frac{1}{Z_sC_s}\sum_j^p \beta\mu_j^{\text{ex}}z_jc_j^{\infty}\right)\\ &+ \frac{\beta\mu_i^{\text{ex}}z_ic_i^{\infty}}{Z_sC_s}, \quad i = 1,\ldots,p.\end{aligned} \tag{18}$$

The zeroth order solution can be obtained by setting $\mu_i^{\text{ex}} = 0$,

$$x_i^0 = \frac{z_i^2 c_i^\infty}{\sum_{j=1}^{p} z_j^2 c_j^\infty} \qquad i = 1, \ldots, p. \tag{19}$$

We conclude this section with the following observation: Combining Eqs. (8) and (14), we can write

$$c_i^{\text{bulk}} = c_i^\infty e^{-\beta\mu_i^{\text{ex}}} X^{z_i} \qquad i = 1, \ldots, p,$$

and we define $v_{\text{shift}} = -\ln(X)/\beta$ to write the previous equation as follows:

$$c_i^{\text{bulk}} = c_i^\infty e^{-\beta z_i v_{\text{shift}} - \beta\mu_i^{\text{ex}}} \qquad i = 1, \ldots, p.$$

This form shows that the correspondence condition described by Eqs. (12) and (13) is equivalent to a potential shift in the original P–BE. Consequently, the electrolyte concentrations in PBCs can be written as follows:

$$c_i^{\text{PBC}}(\mathbf{r}) = c_i^\infty \lambda(\mathbf{r}) e^{-\beta z_i (v(\mathbf{r}) + v_{\text{shift}})} \qquad i = 1, \ldots, p. \tag{20}$$

Eq. (20) is similar to the method of Lagrange multipliers described in detail by Melander *et al.*[16] if the excess chemical potentials are chosen to be proportional to the charge of the electrolyte species,

$$\mu_i^{\text{ex}} = -z_i v_{\text{shift}} \qquad i = 1, \ldots, p. \tag{21}$$

For a binary anti-symmetric electrolyte ($z_+ = -z_-$), this becomes exactly equivalent to the formulation of anti-symmetric excess chemical potentials given by Eq. (35) of Melander *et al.*[16] and Eq. (17) of Gunceler *et al.*[13] Our approach generalizes this type of neutralization, and it establishes physical grounds through the correspondence between OBCs and PBCs. Furthermore, our approach yields a new type of jellium neutralization, as described in Sec. III B.

B. NECS for linearized P–BE

We show in the following that the linearization of the Boltzmann term with shifted concentrations leads to a new type of jellium neutralization and a correction to the Debye length. We start from the linear approximation of the Boltzmann term in the electrolyte charge concentration,

$$\begin{aligned}
&\sum_i^p \lambda(\mathbf{r}) z_i c_i^{\text{bulk}} e^{-\beta z_i v(\mathbf{r}) + \beta\mu_i^{\text{ex}}} \\
&\quad = \sum_i^p \lambda(\mathbf{r}) z_i \left(c_i^\infty - x_i \frac{Z_s C_s}{z_i} \right) e^{-\beta z_i v(\mathbf{r}) + \beta\mu_i^{\text{ex}}}, \qquad (22) \\
&\quad \approx \sum_i^p \lambda(\mathbf{r}) z_i \left(c_i^\infty - x_i \frac{Z_s C_s}{z_i} \right) \left(1 - \beta(z_i v(\mathbf{r}) - \mu_i^{\text{ex}}) \right) \\
&\quad = -Z_s C_s \lambda(\mathbf{r}) - \beta\lambda(\mathbf{r}) \sum_i^p z_i^2 c_i^\infty \left(1 - x_i \frac{Z_s C_s}{z_i c_i^\infty} \right) v(\mathbf{r}), \qquad (23)
\end{aligned}$$

where we have used the fact that for the linearized P–BE, the chemical potential can be absorbed in the electrostatic potential by a uniform shift[18] if the condition $\int_V \lambda(\mathbf{r}) v(\mathbf{r}) d\mathbf{r} = 0$ is satisfied. The shift parameters, $\{x_i\}$, are given by Eq. (14) or Eq. (19).

We note that the integral over the computational cell of the zero order term in Eq. (23) is the solute charge $-Z_s$; hence, we can introduce the "accessible jellium" neutralization for the solute as follows:

$$\rho_{\text{tot}}^{\text{pbc-acc-jellium}}(\mathbf{r}) = \rho_{\text{tot}}(\mathbf{r}) - Z_s C_s \lambda(\mathbf{r}). \tag{24}$$

The coefficient of $v(\mathbf{r})$ in Eq. (23) defines a corrected Debye length,

$$l_D^{-2} = 4\pi\beta \sum_i^p z_i^2 c_i^\infty \left(1 - x_i \frac{Z_s C_s}{z_i c_i^\infty} \right), \tag{25}$$

which in the case of linear approximation for the shift coefficients $\{x_i^0\}$, Eq. (19), reads

$$l_D^{-2} = l_{D,OBC}^{-2} - 4\pi\beta Z_s C_s \frac{\sum_i^p z_i^3 c_i^\infty}{\sum_i^p z_i^2 c_i^\infty}, \tag{26}$$

where $l_{D,OBC}^{-2} = 4\pi\beta \sum_i^p z_i^2 c_i^\infty$. The previous equation shows that the correction is exactly 0 for the two-component symmetric electrolyte (i.e., $z_1 + z_2 = 0$), but, in general, the Debye length varies as a function of the sign of Z_s and the sign of the sum $\sum_i^p z_i^3 c_i^\infty$.

We note that the uniform jellium neutralization, Eq. (6), is a particular case of this derivation for which $\lambda(\mathbf{r}) = 1$ and $\sum_i^p z_i^3 c_i^\infty = 0$.

C. "Accessible jellium" approximation for P–BE

At this point, we can analyze the relationship between neutralization by electrolyte concentration shift (NECS) and the jellium neutralization for the full P–BE. We do this by adding and subtracting the accessible jellium term in the rhs of Eq. (1), expanding the average densities $\{c_i^{\text{bulk}}\}$, and regrouping the terms as follows:

$$\begin{aligned}
&\rho(\mathbf{r}) + \lambda(\mathbf{r}) \sum_i^p z_i c_i^{\text{bulk}} e^{-\beta z_i v(\mathbf{r}) + \beta\mu_i^{\text{ex}}} \\
&\quad = \rho(\mathbf{r}) - Z_s C_s \lambda(\mathbf{r}) + Z_s C_s \lambda(\mathbf{r}) + \lambda(\mathbf{r}) \sum_i^p \\
&\qquad \times (z_i c_i^\infty - x_i Z_s C_s) e^{-\beta z_i v(\mathbf{r}) + \beta\mu_i^{\text{ex}}} \\
&\quad = \rho(\mathbf{r}) - Z_s C_s \lambda(\mathbf{r}) + \lambda(\mathbf{r}) \sum_i^p z_i c_i^\infty e^{-\beta z_i v(\mathbf{r}) + \beta\mu_i^{\text{ex}}} \\
&\qquad + \lambda(\mathbf{r}) Z_s C_s \sum_i^p x_i (1 - e^{-\beta z_i v(\mathbf{r}) + \beta\mu_i^{\text{ex}}}) \\
&\quad = \rho_{\text{tot}}^{\text{pbc-acc-jellium}} + \delta\rho_{\text{shift}}(\mathbf{r}), \qquad (27)
\end{aligned}$$

where

$$\delta\rho_{\text{shift}}(\mathbf{r}) = \lambda(\mathbf{r}) Z_s C_s \sum_i^p x_i (1 - e^{-\beta z_i v(\mathbf{r}) + \beta\mu_i^{\text{ex}}}). \tag{28}$$

Equations (27) and (28) show that the rhs of the P–BE can be written as a sum of the solute charge density (with the new accessibble jellium neutralization), the Boltzmann term, which uses the asymptotic electrolyte densities, $\{c_i^\infty\}$, and a term that involves the concentration shifts $\{x_i\}$. As in the linear case, we note that the standard jellium neutralization can be derived from Eq. (27) by setting $\lambda(\mathbf{r}) = 1$ and dropping the term depending on $\{x_i\}$.

Equation (27) suggests an alternative, "accessible jellium neutralization," in which one replaces the term $(1/V)\int_V \rho_{\text{tot}}(\mathbf{r})d\mathbf{r}$ of Eq. (6) with $Z_s C_s \lambda(\mathbf{r})$ and neglects the term $\delta\rho_{\text{shift}}(\mathbf{r})$. Dropping $\delta\rho_{\text{shift}}(\mathbf{r})$ is an uncontrolled approximation with respect to NECS, but there are two facts that could justify its use in certain cases: (i) $\delta\rho_{\text{shift}}(\mathbf{r}) \propto 1/V_{\text{acc}}$, while the standard Boltzmann term is independent of the computational cell volume; (ii) $|-\beta v(\mathbf{r}) + \beta\mu_i^{\text{ex}}| \ll 1$ far away from the solute; therefore, the product $\lambda(\mathbf{r})(1 - e^{-\beta z_i v(\mathbf{r}) + \beta\mu_i^{\text{ex}}})$ is non-negligible only in the transition region between the excluded and fully accessible domains for the electrolyte ions. A practical advantage of the accessible jellium neutralization approximation is that the computation of the shift parameters $\{x_i\}$ is not needed. The validity of this approximation with respect to NECS will be assessed for several test cases in Sec. IV.

D. Numerical implementation

We have implemented the NECS procedure in the P–BE solver DL_MG[26] as follows: after each evaluation of the excess chemical potential, the concentration shift parameters $\{x_i\}$ are computed from Eq. (14), where the parameter X is found from Eq. (15). For a two-component symmetric electrolyte ($z_1 + z_2 = 0$), Eq. (15) can be reduced to a quadratic equation. For the remaining cases, a one-dimensional Newton method is used to solve it with initial guess given by Eq. (17). The starting values of $\{x_i\}$ at the start of DL_MG solver iterations are computed with Eq. (19).

Besides the NECS neutralization, the DL_MG application interface provides the user with the option to use either of the following: linear approximation [Eq. (16)], accessible jellium neutralization [Eq. (24)], or a user provided set of shift parameters $\{x_i\}$.

IV. RESULTS AND DISCUSSION

We compare the three different solute neutralization schemes that we have presented and implemented here: jellium, accessible jellium, and NECS. We show what effect each of these schemes has on the concentration profiles of electrolyte in PBCs, its deviation from

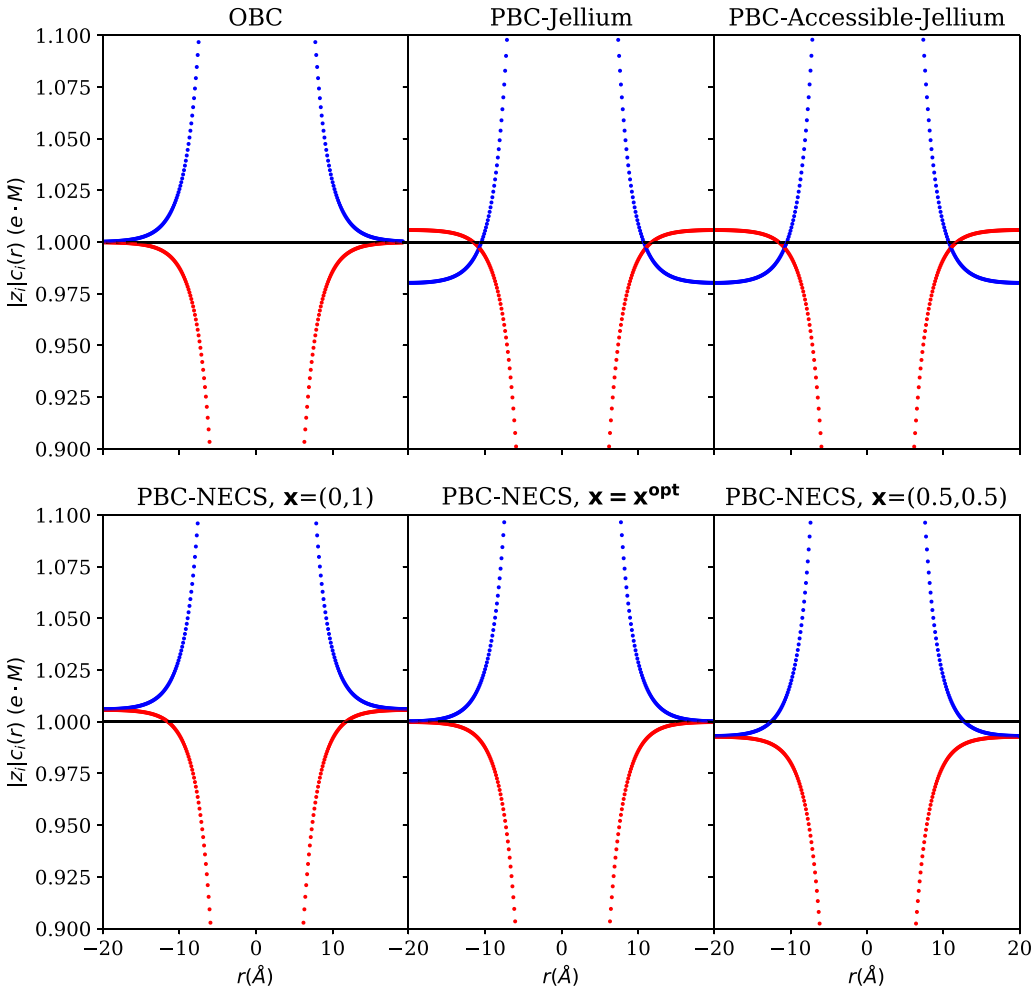

FIG. 2. Concentration profiles for Boltzmann ions in OBCs and with different neutralization schemes in PBCs for a K^+ ion in 0.5M A_2B electrolyte. Red: positive electrolyte A. Blue: negative electrolyte B.

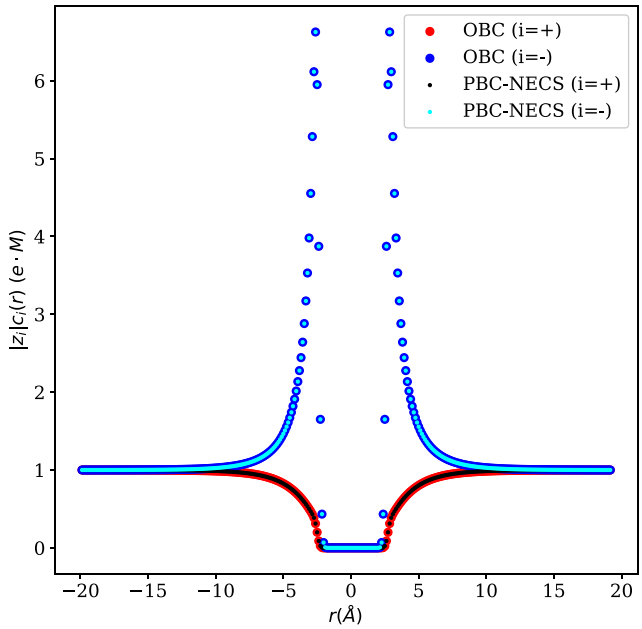

FIG. 3. Direct comparison of concentration profiles for positive (i = +) and negative (i = −) Boltzmann ions in OBCs with NECS ($\mathbf{x} = x^{opt}$) along a straight line containing the K^+ ion placed at the center of a unit cell in 0.5M A_2B electrolyte.

OBCs, asymptotic deviations far away from the quantum system, and total free energy of the system.

A. Single K^+ cation solute

We start our analysis with the simple case of a single K^+ ion as the solute immersed in an electrolyte solution with PBCs. Although this is not a natural periodic system, it is useful to illustrate the correspondence of concentrations of electrolytes between PBCs and OBCs. We place the K^+ in a 0.5M aqueous A_2B-type electrolyte at 298 K at the center of a simulation cell of size 40 × 40 × 40 $Å^3$. The NGWF radius is set to 8.0 a_0 (≈4.2 Å), and the kinetic energy cutoff for the psinc basis set is 1000 eV. We perform this calculation in OBCs as well as PBCs. For PBCs, we examine all the three neutralization schemes: jellium, accessible jellium, and NECS. Within NECS, we show the results for arbitrary shift parameters $\mathbf{x} = \{x_i\}$ as well as for the optimal solution $\mathbf{x}^{opt}$ found using Eqs. (14) and (15). The concentration profiles for Boltzmann ions in OBCs and in PBCs with different neutralization schemes are shown in Fig. 2 along a straight line with K^+ at the origin. We see that in the case of OBCs, the concentration of the Boltzmann ions asymptotically reaches $\{c_i^\infty\}$ at the faces of the box. In the case of jellium and accessible jellium, far away from the K^+ ion, the electrolyte becomes non-neutral, which is unphysical. In the case of NECS, we show the effect of the shift parameters ($\mathbf{x}$). We see that for the simple guesses $\mathbf{x}$ = (0, 1) or $\mathbf{x}$ = (0.5, 0.5), the concentration profiles do not reach the asymptotic value of $\{c_i^\infty\}$, and only the optimal solution $\mathbf{x}^{opt}$ yields concentrations that reach the correct asymptotic limit. For this case, $\mathbf{x}^{opt}$ = (0.226, 0.774). The analytical value predicted from Eq. (18) is $\mathbf{x}^{lin}$ = (0.229, 0.771), which is quite close to the optimal solution. The zeroth order solution from Eq. (19) is $\mathbf{x}^0$ = (0.333, 0.667), which is farther away from the optimal solution. We show a direct comparison between OBCs and NECS ($\mathbf{x} = x^{opt}$) along a straight line containing the K^+ ion in Fig. 3. The similarity between the profiles of OBCs and NECS demonstrates the principle of correspondence between the two. Even though the profiles look exactly the same between OBCs and NECS, there is a minute difference in the actual values; the total electrolyte charge in OBCs integrates to −1.011 68 e, while in NECS, it integrates to −1 e, required to achieve electroneutrality with the quantum K^+ ion.

The corresponding electrostatic potential profiles are shown in Fig. 4. We note that the electrostatic potential in OBCs reaches zero at the boundary following the asymptotic condition [as $\mathbf{r} \to \infty, v(\mathbf{r}) \to 0, c_i(\mathbf{r}) \to c_i^\infty$]. While in NECS in PBCs, there is a potential shift, corresponding to Eq. (20), which shifts the concentrations of electrolyte ions to achieve electroneutrality. We note that

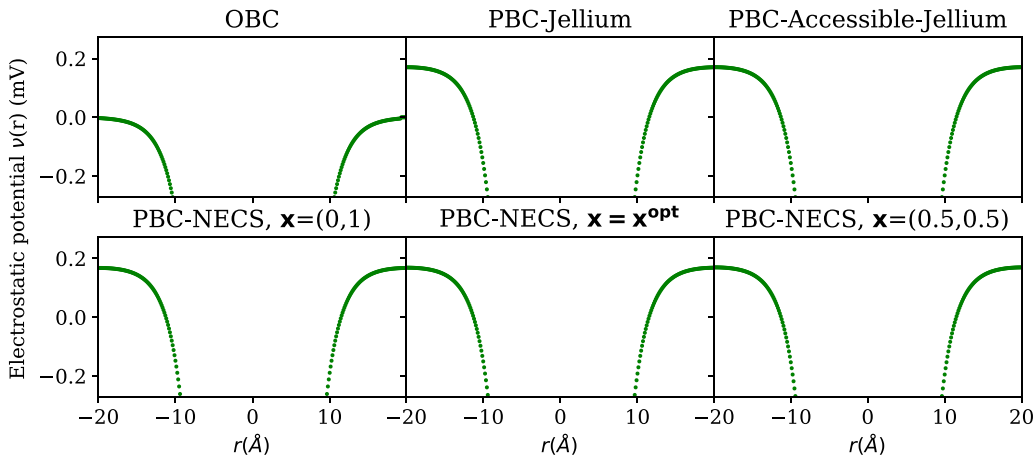

FIG. 4. Electrostatic potential in OBCs and with different neutralization schemes in PBCs for a K^+ ion in 0.5M A_2B electrolyte.

TABLE I. Free energy components (kcal/mol) with different schemes for charge neutrality and their comparison with OBCs.

Energy components	OBCs[a]	Jellium	Ac. jellium	NECS(x^{opt})
Electrostatic energy $\frac{1}{2}\int_V \rho_{tot}^{pbc}(\mathbf{r})v(\mathbf{r})d\mathbf{r}$	3 525.811	3 525.787	3 525.814	3 525.812
Accessibility repulsion energy $k_B T \sum_{i=1}^{p} \int_V c_i(\mathbf{r}) \ln\lambda(\mathbf{r})d\mathbf{r}$	0.025	0.024	0.025	0.025
Osmotic pressure contribution $-k_B T \sum_{i=1}^{p} \int_V c_i(\mathbf{r})d\mathbf{r}$	−32.197	−34.197	−34.197	−34.293
Entropic contribution $k_B T \sum_{i=1}^{p} \int_V c_i(\mathbf{r}) \ln(c_i(\mathbf{r})/c^\circ)d\mathbf{r}$	−7.364	−7.786	−7.786	−7.847
Chemical potential contribution $-\sum_{i=1}^{p} \int_V \mu_i c_i(\mathbf{r})d\mathbf{r}$	7.578	7.996	7.996	8.056
DFT energy	−21 403.450	−21 403.508	−21 403.476	−21 403.476
Cavitation energy	5.967	5.967	5.967	5.967
Dispersion–repulsion energy	−4.290	−4.290	−4.290	−4.290
Total grand potential (Ω)	−17 907.921	−17 910.007	−17 909.948	−17 910.045

[a]Due to difference in boundary conditions in OBCs and PBCs, the finite difference multigrid is 329 × 329 × 329 in OBCs and 336 × 336 × 336 in PBCs.

the electrostatic potential is quite similar for different neutralization schemes in this case.

The individual energy components from OBCs and from different neutralization schemes in PBCs are shown in Table I. We see that, energetically, the accessible jellium neutralization is very similar to the neutralization by electrolyte concentration shift (NECS) and OBCs in comparison of the electrostatic, accessibility, and DFT energy components, while jellium and accessible jellium are similar in comparison of the remaining energy components. All schemes have the same cavitation and dispersion–repulsion energies as these depend only upon the solvent cavity and are not affected by electrolyte concentrations. We note here that the osmotic pressure depends upon the total amount of electrolyte [as $\sum_i \int_V c_i(\mathbf{r})d\mathbf{r} = \sum_i V_{acc} c_i^{bulk}$]; hence, it is the same for jellium and accessible jellium. For NECS, the total amount of electrolyte changes to maintain electroneutrality, while for OBCs, the electroneutrality does not matter. Overall, the total grand potential is quite similar between the three neutralization schemes, while it is different for OBCs, majorly due to the difference in osmotic pressure for this finite system. With the insights obtained from the study of electrolyte concentrations and energy components for a finite system of a single K^+ ion in electrolyte solution, we next focus on truly periodic (extended) systems such as a graphene sheet with a Na^+ atom adsorbed on it and a charged graphite slab.

B. Graphene with adsorbed Na^+ ion

We next turn to a simple extended system—a Na^+ cation adsorbed on graphene, immersed in three electrolytes in sequence: AB, A_2B, and AB_2, all at a 1M concentration. The size of the simulation cell along the graphene sheet is 17.16 × 17.33 Å^2, and two different sizes are considered in the normal direction: 31.75 Å ("smaller cell") and 91.75 Å ("larger cell"). PBC are employed in all directions, making the positioning of the system along the x–y plane irrelevant. The positioning along z, on the other hand, is relevant, since we will be examining the electrolyte ion concentrations at the top and bottom faces of the cell. The system is positioned with the graphene

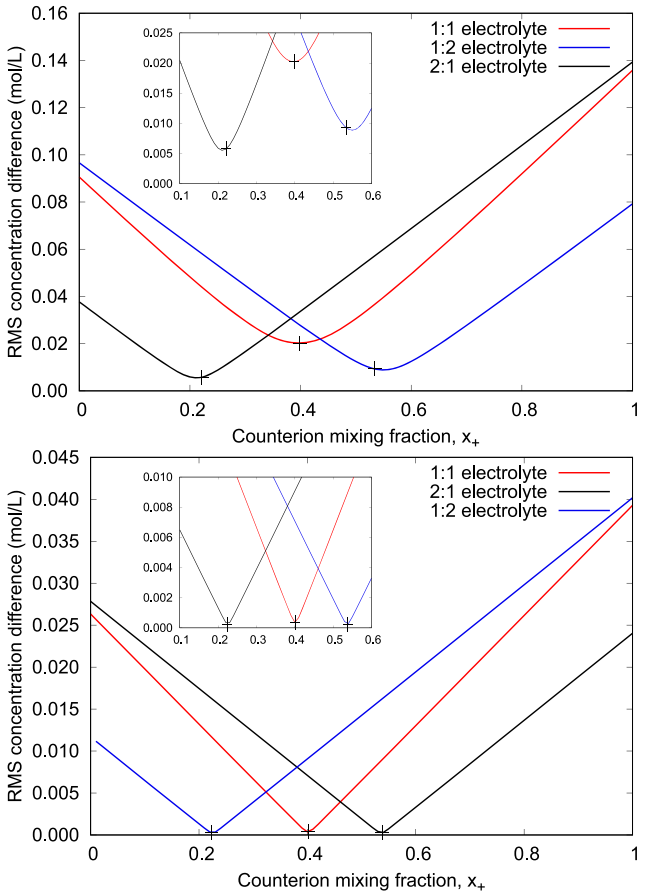

FIG. 5. rms difference in electrolyte ion concentration, relative to the bulk concentration, on the faces of the simulation cell parallel to the graphene sheet (lower is better). Top: smaller cell (17.16 × 17.33 × 31.75 Å^3). Bottom: larger cell (17.16 × 17.33 × 91.75 Å^3). Crosses denote the values obtained from $x_+ = x_+^{opt}$.

sheet in the middle of the cell height. We set the NGWF radius to 7.0 a_0 (≈3.7 Å) and the kinetic energy cutoff to 814 eV.

We first examine the performance of NECS with varying values of the shift parameters **x**. Given that we have a two-component electrolyte, we can introduce the notation $\mathbf{x} = (x_+, x_-)$ for the sake of brevity and work only with x_+ since $x_- = 1 - x_+$.

As shown in Sec. IV A (Fig. 2), an optimal choice of the shift parameters **x** [determined from Eqs. (14) and (15)] leads to electrolyte ion concentrations tending to their bulk values far away from the system, while arbitrary choices result in the concentrations being shifted. We can thus introduce a more practical measure of assessing the quality of the choice of **x**,

$$\delta^2 = \sum_{i=1}^{p} \frac{1}{S} \int_S (c_i^{\infty} - c_i^{\mathrm{PBC}}(\mathbf{r}))^2 \mathrm{d}\mathbf{r}, \tag{29}$$

where the integration is carried out over the simulation cell faces parallel to the graphene. Analogously, for a system extended in 1D (e.g., a nanowire), we would use four cell faces, and for a system that is not extended (like the isolated cation studied in Sec. IV A), we would use all six. Of course, we retain formal 3D periodicity in all cases.

In contrast to Δ defined by (10), the quantity δ—which is nothing else but the rms difference between the electrolyte ion concentrations obtained in PBCs and the desired bulk concentration values—can be easily calculated at every energy evaluation. Having first run a set of calculations with varying x_+ (in increments of 0.01), in Fig. 5, we plot the values of δ for the two system sizes (top and bottom panels) and the three types of electrolyte (curves within each panel). Crosses denote the optimal values determined from Eqs. (14) and (15). As expected, the rms concentration difference is much smaller in the larger cell, where the faces over which it is calculated are farther away from the system. The calculated x_+^{opt} matches the actual minima of the curves to a very good accuracy (this is best seen in the insets).

We will now examine if and how the choice of the neutralization method affects the total charge density due to the electrolyte. For the same Na^+:graphene system in the smaller cell, we ran calculations using neutralization with the jellium, accessible jellium, and NECS approaches. In Fig. 6, we plot the electrolyte charge density in a 2D slice taken along the x–z plane with the y coordinate set to that of the Na^+ ion. We note the following features of interest.

First, NECS predicts a larger net anionic charge density at the point of contact of the Na^+ and graphene exclusion regions. Accessible jellium neutralization does reproduce this to a degree, while jellium predicts smaller concentrations. This is best seen by examining the +0.002 isocontour. Second, jellium and accessible jellium predict small but measurable net *cationic* charge density in the regions further away from the system. Under the convention employed in the plot, this corresponds to regions below the graphene layer and at the top of the plot, where isocontours with small negative values can be

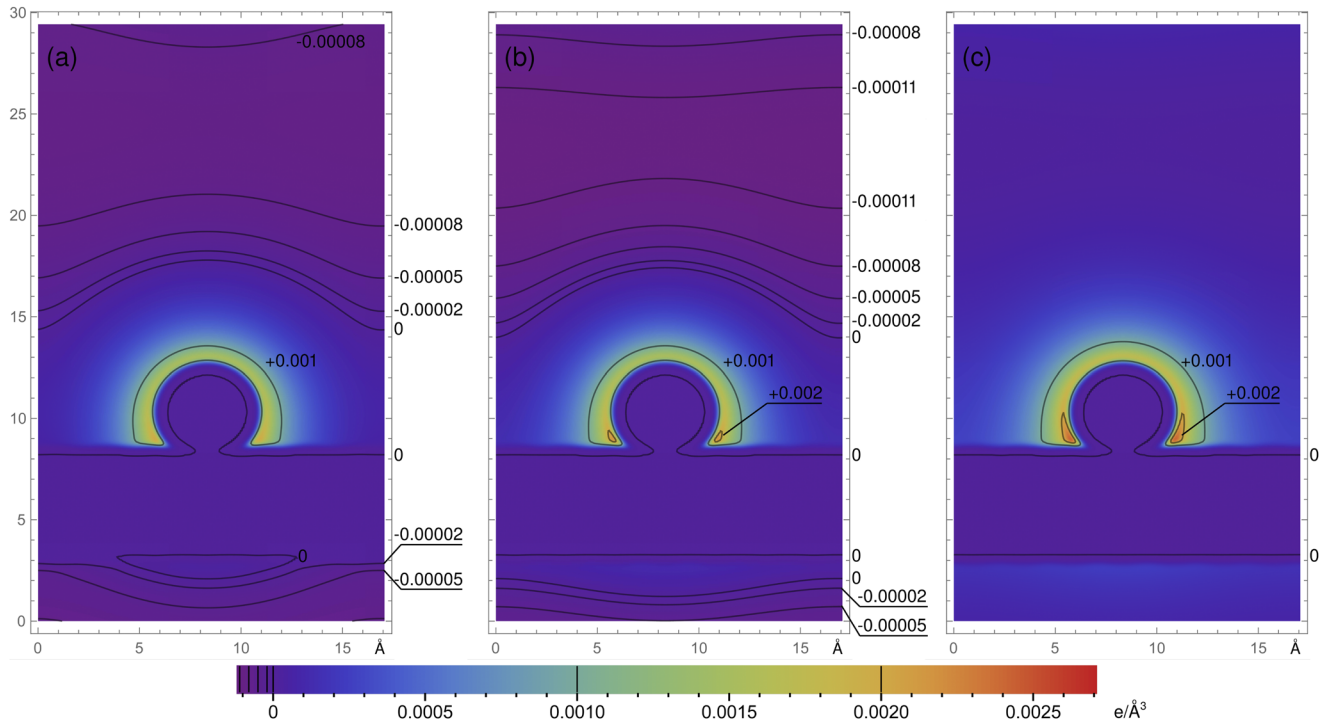

FIG. 6. Total charge density (e/Å^3) of the electrolyte in three charge neutralization models: (a) jellium, (b) accessible jellium, and (c) NECS with $\mathbf{x} = \mathbf{x}^{opt}$ in a x–z plane cross section through the Na^+ ion. For clarity of presentation, anionic charge is shown as positive (warm colors), and the system has been shifted to position the graphene closer to the bottom. The uniform background charge of jellium models is not shown.

seen. NECS, in contrast, predicts the net charge density to be strictly zero or anionic everywhere.

C. Charged graphite electrode

Finally, we test the different neutralization schemes on a model of a charged graphite electrode, which is exposed to the electrolyte along edge planes, as would be expected for the anode of a Li-ion battery. An AA-stacked H-terminated graphite slab ($C_{240}H_{32}$) with a charge of +2 is placed in a 0.5M AB-type electrolyte, within an orthorhombic simulation cell of dimensions 13.763 × 8.535 × 77.247 Å^3, as shown schematically in Fig. 7. The solvent is ethylene carbonate (EC) with a bulk permittivity of 90.7 at 308 K. We use NGWF radii of 8.0 a_0 (≈4.2 Å) with four NGWFs on each C atom and a psinc basis set kinetic energy cutoff of 1000 eV. The planar-averaged concentration profiles of Boltzmann ions [$c_i(z)$, $i = \pm$] are compared in Fig. 7 for jellium, accessible jellium, and NECS with the optimal shift parameters ($\mathbf{x}^{opt}$) found using Eqs. (14) and (15). We can observe a build-up of negative electrolyte (blue) and a depletion of positive electrolyte (red) at the graphite electrolyte interface for all three neutralization schemes, resembling the formation of electric double layers near electrode–electrolyte interfaces. The electrolyte concentration at the interfacial plane peaks to as high as above 4M in case of NECS ($\mathbf{x} = x^{opt}$), while it is around 3M for accessible jellium and around 2M for jellium neutralization. Thus, NECS neutralization correctly captures the physical process of charge storage at the interface.

In the case of jellium and accessible jellium schemes, the charged quantum system (graphite electrode) is neutralized via a fictitious homogeneous background charge, and the electrolyte is self neutral ($c_i^{\text{bulk}} = 0.5\text{M}$, $i = \pm$), which leads to the breaking of electroneutrality ($\sum_i z_i c_i^{\infty} \neq 0$) far away in the bulk electrolyte, seen as a deviation from the green line at extreme z values. In the case of the NECS, there is no fictitious neutralization; the electrolyte bulk concentrations ($c_i^{\text{bulk}}, i = \pm$) are allowed to vary so as to neutralize the quantum system (graphite electrode) and at the same time reach the correct asymptotic limit ($c_i^{\infty} = 0.5\text{M}$, $i = \pm$) in the bulk electrolyte. The optimal solution for this case is $\mathbf{x}^{opt} = (0.240, 0.760)$. The analytical value predicted from the linearized equation (18) [$\mathbf{x}^{lin} = (0.364, 0.636)$] does not strictly coincide with the full non-linear optimal solution ($\mathbf{x}^{opt}$). The zeroth order solution from Eq. (19) is $\mathbf{x}^0 = (0.5, 0.5)$, which is farther away from the optimal solution.

We compare the electrostatic potential for the three neutralization schemes in Fig. 8. The Debye length is 4.7 Å, which is quite smaller than the size of the simulation cell (77.247 Å). From the plot, we see that the profiles of electrostatic potential for the case of accessible jellium and NECS ($\mathbf{x} = \mathbf{x}^{opt}$) become flat much closer to the graphite surface than the jellium neutralization. This indicates an accumulation of counter-charge at the interface for the NECS method, which is not seen to the same extent in jellium neutralization.

We also compare the energy components from different neutralization schemes, as shown in Table II. We observe that the electrostatic energy, DFT energy, and the total grand potential are very similar between accessible jellium and NECS most likely because accessible jellium stems out from applying NECS to linearized P–BE. However, the predictions of the conventional jellium model are quite different in all the three aforementioned free energy components. We further observe that the osmotic pressure component is

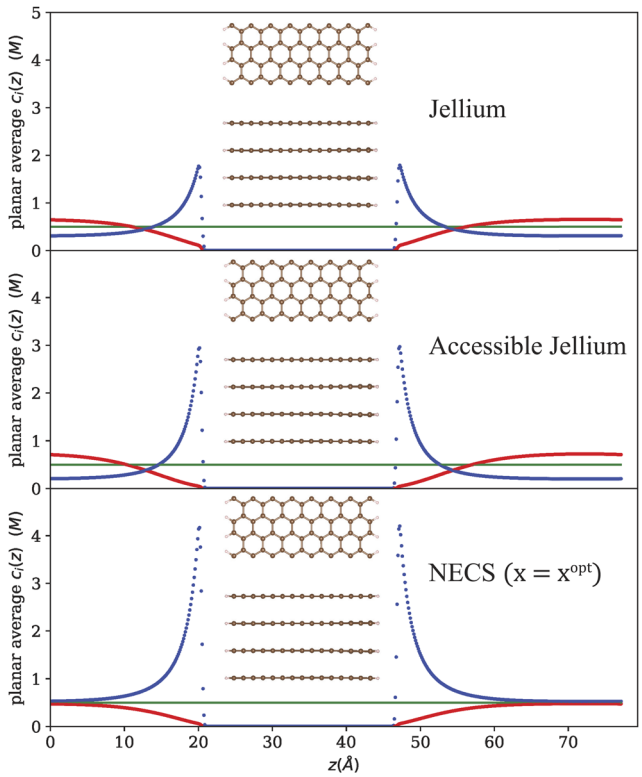

FIG. 7. Concentration profiles for Boltzmann ions with different neutralization schemes for a graphite slab with +2 charge in 0.5M AB-type electrolyte. Color scheme: red: positive electrolyte A, blue: negative electrolyte B, and green: asymptotic value of 0.5M concentration. The top and front views of AA-stacked H-terminated graphite slab ($C_{240}H_{32}$) are shown.

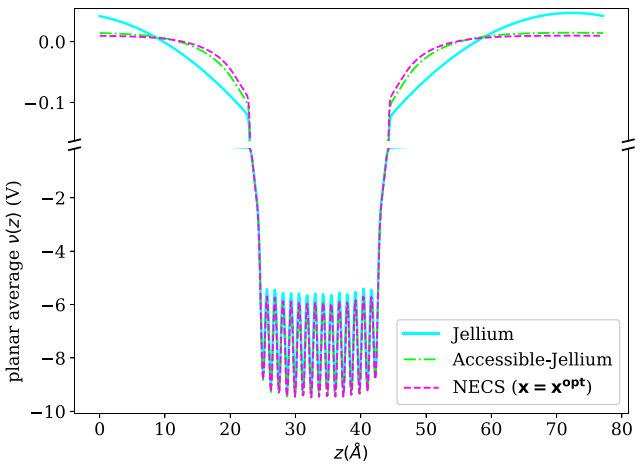

FIG. 8. Planar average electrostatic potential with different neutralization schemes for the graphite slab with +2 charge in 0.5M AB-type electrolyte.

TABLE II. Free energy components (kcal/mol) with different schemes for the charged graphite–electrolyte interface.

Energy components	Jellium	Acc. jellium	NECS(x^{opt})
Electrostatic energy $\frac{1}{2}\int_V \rho_{tot}^{pbc}(\mathbf{r})v(\mathbf{r})d\mathbf{r}$	148 982.432	148 944.742	148 944.566
Accessibility repulsion energy $k_B T \sum_{i=1}^{p} \int_V c_i(\mathbf{r}) \ln\lambda(\mathbf{r})d\mathbf{r}$	0.025	0.043	0.060
Osmotic pressure contribution $-k_B T \sum_{i=1}^{p} \int_V c_i(\mathbf{r})d\mathbf{r}$	−2.200	−2.200	−2.836
Entropic contribution $k_B T \sum_{i=1}^{p} \int_V c_i(\mathbf{r}) \ln(c_i(\mathbf{r})/c^\circ)d\mathbf{r}$	−1.285	−0.935	−0.462
Chemical potential contribution $-\sum_{i=1}^{p} \int_V \mu_i c_i(\mathbf{r})d\mathbf{r}$	1.778	2.126	1.456
DFT energy	−1 026 071.506	−1 025 950.769	−1 025 950.770
Cavitation energy	30.844	30.844	30.844
Dispersion–repulsion energy	−22.174	−22.174	−22.174
Total grand potential (Ω)	−877 082.087	−876 998.323	−876 999.316

identical for the two jelliums due to the same total electrolyte charge in the simulation cell [$\sum_i \int_V c_i(\mathbf{r})d\mathbf{r} = \sum_i V_{acc} c_i^{bulk}$], whereas different for NECS as the amount of electrolyte is varied to achieve electroneutrality.

V. CONCLUSIONS

We have developed a new scheme for DFT calculations of charged materials (e.g., electrodes) in periodic boundary conditions (PBCs) within the Poisson–Boltzmann electrolyte model where electrical neutrality is achieved via the electrolyte, as in real experiments. Our new method of neutralization by electrolyte concentration shift (NECS) neutralizes the quantum charge directly by electrolyte charge and allows the asymptotic electrolyte concentrations to reach their bulk values, in contrast with the commonly employed neutralization by a uniform background charge (jellium). Our approach is based on a principle of correspondence of the PBC concentration profiles with those under open boundary conditions that leads to the correct asymptotic concentrations, something that we demonstrated also numerically for the case of a K^+ cation. In further tests, we systematically scanned across a range of shifted bulk concentrations for a Na^+–graphene system and showed that the NECS approach produces the most physical results. Furthermore, the application of NECS for the linearized P–BE led to a new kind of jellium-like neutralization within the electrolyte accessible region. This "accessible jellium" model is an improvement over conventional jellium and simpler to implement than NECS. All the neutralization schemes were finally tested on a charged graphite system (a simple electrode model), which is relevant for electrochemical applications. We have found that the jellium-based models break electroneutrality in the bulk electrolyte, while concentration profiles obtained with NECS reach the correct asymptotic limits and produce a realistic description of the behavior of electrolyte around charged interfaces. We expect the NECS model, which we have implemented in the ONETEP linear-scaling DFT code for large-scale DFT calculations, will enable accurate simulations in technologically important areas such as Li-ion batteries and electrocatalysis.

ACKNOWLEDGMENTS

This work was carried out with funding from the Faraday Institution (faraday.ac.uk; No. EP/S003053/1), Grant No. FIRG003. The majority of computations presented in this work were performed on the Iridis5 supercomputer of the University of Southampton and the Michael supercomputer of the Faraday Institution. We acknowledge the UK Materials and Molecular Modelling Hub for computational resources, partially funded by the EPSRC (Grant No. EP/P020194/1). J.D. also acknowledges support from the EPSRC (Grant No. EP/P02209X/1). J.D. acknowledges the support of the TASK Academic Computer Centre (Gdańsk, Poland), where some of the calculations were run. We would like to thank Professor John Owen of the University of Southampton for helpful discussions.

DATA AVAILABILITY

The data that support the findings of this study are available within the article.

REFERENCES

[1] J. C. A. Prentice *et al.*, "The ONETEP linear-scaling density functional theory program," J. Chem. Phys. **152**, 174111 (2020).
[2] M. H. Hansen and J. Rossmeisl, "pH in grand canonical statistics of an electrochemical interface," J. Phys. Chem. C **120**, 29135–29143 (2016).
[3] S. Sakong, M. Naderian, K. Mathew, R. G. Hennig, and A. Groß, "Density functional theory study of the electrochemical interface between a Pt electrode and an aqueous electrolyte using an implicit solvent method," J. Chem. Phys. **142**, 234107 (2015).
[4] R. E. Skyner, J. L. McDonagh, C. R. Groom, T. Van Mourik, and J. B. O. Mitchell, "A review of methods for the calculation of solution free energies and the modelling of systems in solution," Phys. Chem. Chem. Phys. **17**, 6174–6191 (2015).
[5] J. Kang, S.-H. Wei, K. Zhu, and Y.-H. Kim, "First-principles theory of electrochemical capacitance of nanostructured materials: Dipole-assisted subsurface intercalation of lithium in pseudocapacitive TiO_2 anatase nanosheets," J. Phys. Chem. C **115**, 4909–4915 (2011).

[6]T. Dufils, G. Jeanmairet, B. Rotenberg, M. Sprik, and M. Salanne, "Simulating electro chemical systems by combining the finite field method with a constant potential electrode," Phys. Rev. Lett. **123**, 195501 (2019).
[7]R. Jorn, R. Kumar, D. P. Abraham, and G. A. Voth, "Atomistic modeling of the electrode–electrolyte interface in Li-ion energy storage systems: Electrolyte structuring," J. Phys. Chem. C **117**, 3747–3761 (2013).
[8]C. Zhang, T. Sayer, J. Hutter, and M. Sprik, "Modelling electrochemical systems with finite field molecular dynamics," J. Phys.: Energy **2**, 032005 (2020).
[9]C. J. Cramer and D. G. Truhlar, "Implicit solvation models: Equilibria, structure, spectra, and dynamics," Chem. Rev. **99**, 2161–2200 (1999).
[10]J. Tomasi, B. Mennucci, and R. Cammi, "Quantum mechanical continuum solvation models," Chem. Rev. **105**, 2999–3093 (2005).
[11]P. Grochowski and J. Trylska, "Continuum molecular electrostatics, salt effects, and counterion binding—A review of the Poisson–Boltzmann theory and its modifications," Biopolymers **89**, 93–113 (2008).
[12]R. Jinnouchi and A. B. Anderson, "Electronic structure calculations of liquid-solid interfaces: Combination of density functional theory and modified Poisson–Boltzmann theory," Phys. Rev. B **77**, 245417 (2008).
[13]D. Gunceler, K. Letchworth-Weaver, R. Sundararaman, K. A. Schwarz, and T. A. Arias, "The importance of nonlinear fluid response in joint density-functional theory studies of battery systems," Modell. Simul. Mater. Sci. Eng. **21**, 074005 (2013).
[14]S. Ringe, H. Oberhofer, C. Hille, S. Matera, and K. Reuter, "Function-space-based solution scheme for the size-modified Poisson–Boltzmann equation in full-potential DFT," J. Chem. Theory Comput. **12**, 4052–4066 (2016).
[15]F. Nattino, M. Truscott, N. Marzari, and O. Andreussi, "Continuum models of the electrochemical diffuse layer in electronic-structure calculations," J. Chem. Phys. **150**, 041722 (2019).
[16]M. M. Melander, M. J. Kuisma, T. E. K. Christensen, and K. Honkala, "Grand-canonical approach to density functional theory of electrocatalytic systems: Thermodynamics of solid-liquid interfaces at constant ion and electrode potentials," J. Chem. Phys. **150**, 041706 (2019).
[17]C. J. Stein, J. M. Herbert, and M. Head-Gordon, "The Poisson–Boltzmann model for implicit solvation of electrolyte solutions: Quantum chemical implementation and assessment via Sechenov coefficients," J. Chem. Phys. **151**, 224111 (2019).
[18]J. Dziedzic, A. Bhandari, L. Anton, C. Peng, J. C. Womack, M. Famili, D. Kramer, and C.-K. Skylaris, "A practical approach to large scale electronic structure calculations in electrolyte solutions via continuum-embedded linear-scaling DFT," J. Phys. Chem. C **124**, 7860–7872 (2020).
[19]G. Kastlunger, P. Lindgren, and A. A. Peterson, "Controlled-potential simulation of elementary electrochemical reactions: Proton discharge on metal surfaces," J. Phys. Chem. C **122**, 12771–12781 (2018).
[20]F. G. Donnan, "The theory of membrane equilibria," Chem. Rev. **1**, 73–90 (1924).
[21]M. Otani and O. Sugino, "First-principles calculations of charged surfaces and interfaces: A plane-wave nonrepeated slab approach," Phys. Rev. B **73**, 115407 (2006).
[22]C. K. Skylaris, P. D. Haynes, A. A. Mostofi, and M. C. Payne, "Introducing ONETEP: Linear-scaling density functional simulations on parallel computers," J. Chem. Phys. **122**, 084119 (2005).
[23]C.-K. Skylaris, A. A. Mostofi, P. D. Haynes, O. Diéguez, and M. C. Payne, "Nonorthogonal generalized Wannier function pseudopotential plane-wave method," Phys. Rev. B **66**, 035119 (2002).
[24]A. A. Mostofi, P. D. Haynes, C.-K. Skylaris, and M. C. Payne, "Preconditioned iterative minimization for linear-scaling electronic structure calculations," J. Chem. Phys. **119**, 8842–8848 (2003).
[25]J. C. Womack, L. Anton, J. Dziedzic, P. J. Hasnip, M. I. J. Probert, and C.-K. Skylaris, "A parallel multigrid Poisson and Poisson–Boltzmann solver for electronic structure calculations in vacuum and solution," J. Chem. Theory Comput. **14**, 1412–1432 (2018).
[26]See http://www.dlmg.org for the source code.
[27]J. C. Womack, L. Anton, J. Dziedzic, P. J. Hasnip, M. I. J. Probert, and C.-K. Skylaris, *Implementation and Optimisation of Advanced Solvent Modelling Functionality in CASTEP and ONETEP* (ARCHER eCSE technical report, 2017), http://www.archer.ac.uk/community/eCSE/eCSE07-06/eCSE07-06.php.
[28]J. C. Howard, J. C. Womack, J. Dziedzic, C.-K. Skylaris, B. P. Pritchard, and T. D. Crawford, "Electronically excited states in solution via a smooth dielectric model combined with equation-of-motion coupled cluster," J. Chem. Theory Comput. **13**, 5572–5581 (2017).
[29]M. J. Holst and F. Saied, "Numerical solution of the nonlinear Poisson–Boltzmann equation: Developing more robust and efficient methods," J. Comput. Chem. **16**, 337–364 (1995).
[30]U. Trottenberg, C. W. Oosterlee, and A. Schuller, *Multigrid* (Academic Press, 2001).
[31]J. Dziedzic, S. J. Fox, T. Fox, C. S. Tautermann, and C.-K. Skylaris, "Large-scale DFT calculations in implicit solvent—A case study on the T4 lysozyme L99A/M102Q protein," Int. J. Quantum Chem. **113**, 771–785 (2013).
[32]We note that chemically a solute is something that dissolves in the solvent to form a solution. The DFT+P–BE models were traditionally developed to predict solvation energies of ions; hence, the quantum system was called the solute. We retain this definition to call the quantum system the solute, even when it is a graphite electrode in practice. The term electrolyte is used for continuum Boltzmann ions.
[33]C. C. Lee, "The charge conserving Poisson–Boltzmann equations: Existence, uniqueness, and maximum principle," J. Math. Phys. **55**, 051503 (2014).
[34]L. Wan, S. Xu, M. Liao, C. Liu, and P. Sheng, "Self-consistent approach to global charge neutrality in electrokinetics: A surface potential trap model," Phys. Rev. X **4**, 011042 (2014).